

## Dominating factors of the wave velocity anisotropy for TCDP borehole

Chang-No WU<sup>(1)</sup>, Che-Ming YANG<sup>(1)</sup>, Wen-Jie WU<sup>(1)</sup> and Jia-Jyun DONG<sup>(1)</sup>

(1) Applied Geology Institute, National Central University, Chungli, Taiwan  
E-mail:arnold790222@hotmail.com

### Abstract

The direction of the fast horizontal shear wave velocity (FSH direction) is frequently used as an indication of the direction of the maximum horizontal principal stress. However, together with the stress induced anisotropy, the wave velocity anisotropy will also be dominated by the inherent anisotropy including the effects of sedimentary and tectonic structures. This study carefully evaluates the influence factors of wave velocity anisotropy in Taiwan Chelungpu-Fault Drilling Project (TCDP) borehole. The anisotropic compliance tensors of sandstones and mudrocks were derived from the laboratory wave measurement. The equivalently continue model was used to evaluate the compliance tensor of jointed rocks, which considered the anisotropy distribution of discontinuities. The lithology was identified as the most influential factor on the wave velocity anisotropy. The dip angle of the bedding plan is also a dominating factor. Surprisingly, the joints distributed in the rock mass are not significantly influencing the wave velocity anisotropy. Generally, the measured FSH directions of sandstones can be accounted by the anisotropy of sandstones. When the dip angles are steeper (in a depth greater than 1800 m), the measured FSH directions of siltstones seems dominated by the dip direction of bedding planes. The spatial variations of the FSH direction in siltstones could be related to the low inherent anisotropy. This study demonstrated that determining the direction of the maximum horizontal principal stress from the FSH directions should consider the influence of inherent anisotropy of rock mass base on the TCDP borehole data.

**Keywords:** TCDP, shear wave anisotropy, inherent anisotropy, fast shear wave velocity, maximum horizontal principal stress

### 1. Introduction

The directions of the fast horizontal shear wave velocity (FSH) measured in boreholes are sometimes used as indications of the maximum horizontal principal stress (Boness and Zoback, 2006a). However, the wave velocity anisotropy can orient from the inherent anisotropy of the medium (e.g., alignment of minerals or grains; bedding plane, aligned macroscopic fractures, and faults) in addition to the anisotropic stress state (Alford, 1986; Mueller, 1991; Sayers, 1994; Brie et al., 1998; Boness and Zoback, 2004; Boness and Zoback, 2006b). In this case study, the influence of inherent anisotropy (including bedding planes and joints) on the direction of FSH is quantitatively evaluated. The available data, includes the borehole logging and laboratory testing produced from the Taiwan Chelungpu fault Drilling

Project (TCDP) was used (Lin et al., 2007; Yeh et al., 2007; Wu et al., 2008; Yabe et al., 2008; Louis et al., 2008; 2012; Hung et al., 2009; Haimson et al., 2010). The appropriateness of using the direction of FSH to evaluate the direction of maximum horizontal principal stress will be presented.

### 2. Methodology

In this study, two sources of inherent anisotropy of rock mass were considered, namely: intact rocks (bedding plane and micro-fractures), and joints. Christoffel equation (Musgrave, 1971) was used to link the anisotropic wave velocity and the elastic stiffness (or elastic compliance) of the medium. The coordinate system used is showed in Fig. 1. Axes 1, 2, and 3 represent East, North, and up directions, respectively. Axes 1', 2', and 3' are the dip direction,

strike, and normal directions of the bedding plane of the sedimentary rocks.

### 2.1 Elastic compliance of intact rocks

If the wave velocities parallel and perpendicular to the bedding plane of the intact rocks are available, we can easily obtain the elastic stiffness matrix (in the coordinate system of 1', 2', and 3') as follows:

$$C_{IJ}^{(M)} = \begin{bmatrix} C_{11}^{(M)} & C_{12}^{(M)} & C_{13}^{(M)} & 0 & 0 & 0 \\ C_{21}^{(M)} & C_{22}^{(M)} & C_{23}^{(M)} & 0 & 0 & 0 \\ C_{31}^{(M)} & C_{32}^{(M)} & C_{33}^{(M)} & 0 & 0 & 0 \\ 0 & 0 & 0 & C_{44}^{(M)} & C_{45}^{(M)} & C_{46}^{(M)} \\ 0 & 0 & 0 & C_{54}^{(M)} & C_{55}^{(M)} & C_{56}^{(M)} \\ 0 & 0 & 0 & C_{64}^{(M)} & C_{65}^{(M)} & C_{66}^{(M)} \end{bmatrix} \quad (1)$$

The above elastic stiffness matrix (6\*6) can be expressed as a tensor by Voigt notation  $C_{i'j'k'l'}$  (Musgrave, 1971). Accordingly, the compliance tensor  $S_{i'j'k'l'}$  in the 1'-2'-3' coordinate system can be derived from  $C_{i'j'k'l'}$  easily. After coordinate system transformation, the compliance  $S_{ijkl}$  of the intact rocks in 1-2-3 coordinate system can be obtained.

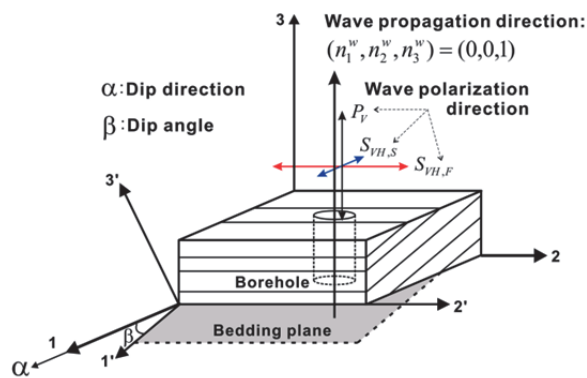


Fig. 1 Coordinate system.

### 2.2 Elastic compliance tensor of jointed rock mass

Oda (1988) proposed an equivalent continuum model for describing the elastic compliance of jointed rock mass. The joints were represented by sets of parallel plates connected by two springs in normal and shear directions. The elastic compliance tensor of the jointed rock mass (excludes the influence of intact

rock) in 1-2-3 coordinate system can be expressed as follows:

$$S_{ijkl}^C = (1/\bar{h} - 1/\bar{g})P_{ijkl} + (1/4\bar{g})(\delta_{ik}P_{jl} + \delta_{jk}P_{il} + \delta_{il}P_{jk} + \delta_{jl}P_{ik}) \quad (2)$$

where  $P_{ij}$ ,  $P_{ijkl}$  are the crack tensors reflected the joints characteristic (i.e. orientation ( $n$ ), the volume density of joint ( $\rho_c$ ) and diameter of joints ( $r$ )), which can be calculated as follows:

$$P_{ij} = (\pi\rho_c / 4) \int_r^m \int_{\Omega} r^3 n_i n_j E(n^c, r) d\Omega dr \quad (3)$$

$$P_{ijkl} = (\pi\rho_c / 4) \int_r^m \int_{\Omega} r^3 n_i n_j n_k n_l E(n^c, r) d\Omega dr \quad (4)$$

The  $\bar{h}$  and  $\bar{g}$  in Eq. (2) represent the averaged normal and shear stiffness, respectively, which can be calculated using Eqs. (5) and (6).

$$\bar{h} = (h + c\sigma_n N_{ij}) \quad (5)$$

$$\bar{g} = g\sigma_n N_{ij} \quad (6)$$

$$N_{ij} = \int_{\Omega} n_i n_j E(n^c) d\Omega \quad (7)$$

The  $h$  and  $g$  in Eqs. (5) and (6) are constants.  $c$  is aspect ratio which is introduced as a measure of crack shape. The ratio is assumed as a constant in this study. The  $N_{ij}$  is a directional density function that describe the probability of the normal vectors in different direction.

### 2.3 The velocity anisotropy of rock mass

To calculate the velocity of rock mass along certain direction, the Christoffel equation (Eq. (8)) can be used.

$$\begin{bmatrix} \Gamma_{11} - \rho V^2 & \Gamma_{12} & \Gamma_{13} \\ \Gamma_{21} & \Gamma_{22} - \rho V^2 & \Gamma_{23} \\ \Gamma_{31} & \Gamma_{32} & \Gamma_{33} - \rho V^2 \end{bmatrix} \begin{bmatrix} U_1 \\ U_2 \\ U_3 \end{bmatrix} = 0 \quad (8)$$

$\Gamma_{ik} = C_{ijkl}^{(R)} n_j^w n_l^w$  is the Christoffel matrix, which is a

function of the wave direction  $n_j^w$  and elastic stiffness tensor of the rock mass  $C_{ijkl}^{(R)}$ . The  $\rho$  and  $V$  represent the density of rock and wave velocity respectively. Based on the eigenvalue  $\rho V^2$  and the eigenvector  $U$ , the wave velocities and the polarized direction of three waves (one is P-wave velocity  $V_p$ , the others are S-waves  $V_s$ ) can be obtained.

## 2.4 Data

The data of sonic wave velocity of host rock we used are from Louis et al. (2008; 2012). They measured the P-wave velocity of the sandstone and siltstone retrieved from TCDP hole A. Based on the measured wave velocity, the siltstone is a transversely isotropic material which is mainly dominated by the bedding plane. Sandstone is orthotropic under atmosphere pressure for the presence of micro fractures normal to the bedding plane. However, with increasing confining pressure, the orthotropic nature gradually transformed into transversely isotropic (Louis et al., 2012). As the results, both siltstone and sandstone are considered as a transversely isotropic material in this study. The measured P-wave velocity of Louis et al. (2008; 2012) was used to evaluate the elastic constants of intact rocks. The required S-wave velocity of sandstone and siltstone was estimated from velocity ratios ( $R = V_p/V_s$ ) of 1.5 and 1.9 (Castagn et al., 1985). Notable, the wave velocities propagating through shales and siltstones are assumed identical and these two rock types are represented as mudrocks in the following analysis. That is, the laboratory wave velocity measurement of siltstones was used to represent the wave velocity of mudrocks.

To determine the parameters of equivalent model (normal vector of joints  $n$  and the volume density of joint  $\rho_c$ ), we use the borehole image of TCDP hole A documented by Wu et al. (2008). The normal stiffness proposed by Cheng (2006) and the shear stiffness proposed by Oda (1988) was used.

To evaluate the velocity anisotropy, the velocity anisotropy ratio  $A$  and FSH direction  $D_{FSH}$  was

used.  $A$  can be calculated as follows:

$$A = 100 * (V_{s-fast}^2 - V_{s-slow}^2) / V_{s-slow}^2 \quad (9)$$

where  $V_{s-fast}^2$  and  $V_{s-slow}^2$  are the fastest and slowest shear wave velocity.

## 3. Results

### 3.1 Observed velocity anisotropy from logging

Fig. 2 shows the measured anisotropy ratio of shear wave velocity  $A$  (purple line, unit: %), and FSH direction  $D_{FSH}$  (red line, unit: degree). The fault zones (e.g. FZA1111, FZA1525, FZA1679) were identified by Yeh et al. (2007) from core analysis data. It can be observed that the  $D_{FSH}$  is influenced by the fault zones. Besides, it is obvious that the changes of  $D_{FSH}$  and  $A$  decrease with increasing depth.

Furthermore, it appears that lithology is a dominating factor of the anisotropy of shear wave velocity. As shown in Fig. 2,  $D_{FSH}$  in sandstone is mostly distributed in  $120^\circ$  and  $A$  decreases with increasing depth. However,  $D_{FSH}$  and  $A$  of siltstone and shale are relatively scattered. The general trend of  $D_{FSH}$  and  $A$  are described as follows:

- (1) The velocity anisotropy ratio  $A$  in sandstone decreases from about 30% to 10% with increasing depth.
- (2) Generally speaking, FSH direction  $D_{FSH}$  in sandstone mostly distributed in  $110^\circ - 120^\circ$ . Above 750 m,  $D_{FSH}$  is relatively scattered, which abruptly approached to north ( $0^\circ$ ) or east ( $90^\circ$ ) than back to  $120^\circ$  soon, especially in 500m – 650m. Right below -1650 m,  $D_{FSH}$  abruptly approached to  $180^\circ$  and gradually decreased to  $60^\circ$ , than back to  $120^\circ$ .
- (3) The velocity anisotropy ratio  $A$  in siltstones and shales (mudrocks) are more scattered than in sandstone. The velocity anisotropy ratio  $A$  is significantly influenced by fault zones. Notable,  $A$  abruptly increases from 10% into 30% below 1785 m.
- (4) Similar to the case of sandstones, FSH direction  $D_{FSH}$  in siltstones and shales are mostly concentrated within  $110^\circ - 120^\circ$ . However, the measured  $D_{FSH}$  for siltstone and shale is relatively scattered. Apparently, the  $D_{FSH}$  is also influenced by the presence of fault zones. Interestingly, at a depth greater than 1785m, the

FSH direction  $D_{FSH}$  concentrated at about  $105^\circ$  (The dip direction of formation). Notable, the dip angle abruptly changed from  $30^\circ$  to about  $60^\circ$  below 1785m (Yeh et al., 2007).

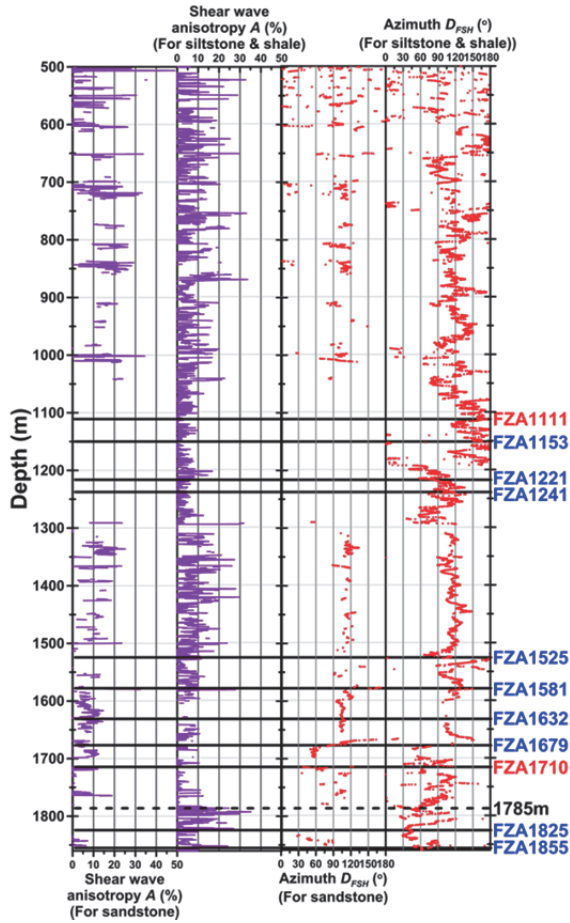


Fig. 2 The shear wave velocity anisotropy of sandstone, siltstone and shale. Purple line represents the velocity anisotropy ratio  $A$ . Red line represents the FSH direction  $D_{FSH}$ . FZA represents fault zone.

### 3.2 Calculated velocity anisotropy neglecting the influence of joints

Based on the Christoffel equation and the elastic compliance matrix of intact rocks (sandstone and mudrock) derived from the wave velocity measured by Louis et al. (2008, 2012), the anisotropy ratio  $A$  and the FSH direction  $D_{FSH}$  on arbitrary plane can be calculated. It is indicated by Louis et al. (2008, 2012) that the anisotropy of intact rocks is mainly dominated by the bedding plane for mudrocks and dominated by the micro fractures which are parallel to the dip direction for sandstones. As aforementioned, the orthotropic nature of sandstones transformed gradually into transversely isotropic nature when the confining stress increased. The studied rocks are

assumed as transversely isotropic materials. The isotropic plane of mudrock is bedding plane while that of the sandstone is the micro fracture which is perpendicular to the bedding plane. That is, the anisotropy of sandstone is only dominated by the micro fractures. Since the shear wave velocities of sandstones are confining stress sensitive, the pressure dependent nature of sandstone was considered.

The elastic compliance tensor was derived from the measured P-wave velocity (Louis et al., 2008; 2012) and the estimated S-wave velocity (from the velocity ratios ( $R = V_p / V_s$ )). Based on the inferred elastic compliance tensor, the  $A$ ,  $D_{FSH}$ , fastest and slowest shear velocity ( $S_{VH,F}$  and  $S_{VH,S}$ ) of siltstone and sandstones can be calculated by Eq. (8). Fig. 3 shows  $S_{VH,F}$  and  $S_{VH,S}$  of siltstone with different dip angles, which propagating in vertical direction and polarized in horizontal direction. The red and blue lines represent the fastest and slowest shear wave velocities. The pink line is the velocity anisotropy ratio  $A$ . From Fig. 3,  $A$  of siltstone is increased with increasing dip angle. Notable,  $A$  is low ( $\sim 5\%$ ) when the dip angle below 30 degree.  $A$  of sandstone will not be influenced by the dip angle of bedding plane for the normal of the micro fractures is on the horizontal plane. However, the  $D_{FSH}$  will be identical to the dip direction of the bedding plane since the strike of the micro fractures is parallel to the dip direction. Meanwhile, the velocity anisotropy ratio of sandstone is decreased with confining stress (Fig. 4) where a lower law is assumed to represent the stress dependence (Louis et al., 2012).

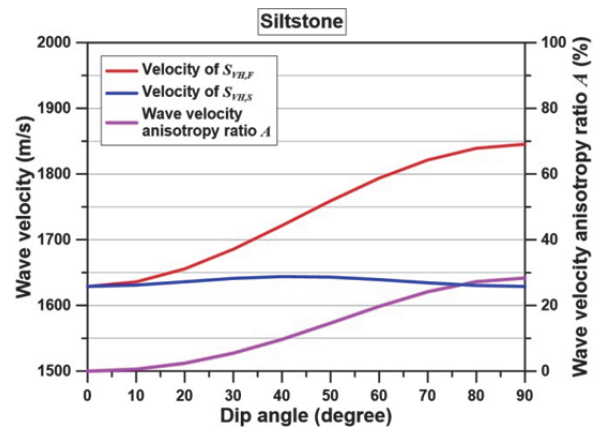


Fig. 3 Shear wave velocity anisotropy changes with dip angle in siltstone.

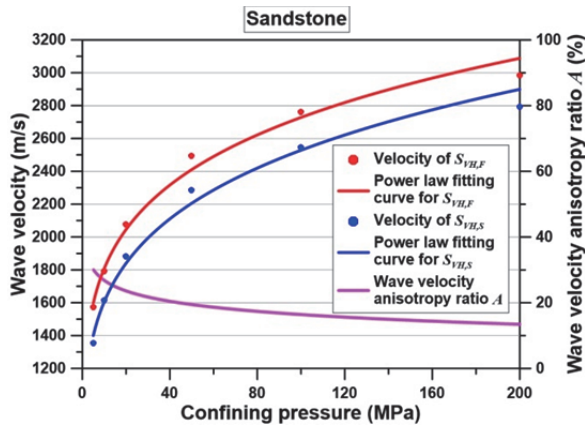


Fig. 4 Shear wave velocity anisotropy changes with confining pressure in sandstone.

Yeh et al. (2007) documented that the dip direction is  $105^\circ$ . The dip angle is about 30 degree above 1710 m and 60 degree below 1710 m. The calculated and measured anisotropic shear wave velocities are shown in Fig. 5. It is obvious that  $D_{FSH}$  and  $A$  of sandstone are decreased with increasing depth. The spatial variation is insignificant. That is, the anisotropy of sandstones is well depicted based on the elastic compliance of intact rock. However, in mudrock, there is a significant mismatch between the predicted and measured anisotropy. It indicated that other factors such as joints or in-situ stress could dominate the anisotropy. Notable, the predicted results in depth below 1785 m of mudrocks are closed to the measured ones. The dip angle abruptly increased from  $30^\circ$  to  $60^\circ$  (Yeh et al., 2007) could account for the good prediction. That is, the wave anisotropy below 1785m is mainly dominated by dip angle.

### 3.3 Calculated velocity anisotropy considering the influence of joints

Wu et al. (2008) reported TCDP core image. Accordingly, the joint orientations required for Oda's equivalent model are available and the anisotropic characteristics of the elastic wave of rock mass around TCDP hole-A. Six depth intervals were selected with uniform lithology to calculate the  $D_{FSH}$  and  $A$ . The results are summarized in Table 1. The influence of joints on the anisotropy of sandstone and mudrock is insignificant. It is reasonable for the anisotropy induced by joints will decrease with increasing depth.

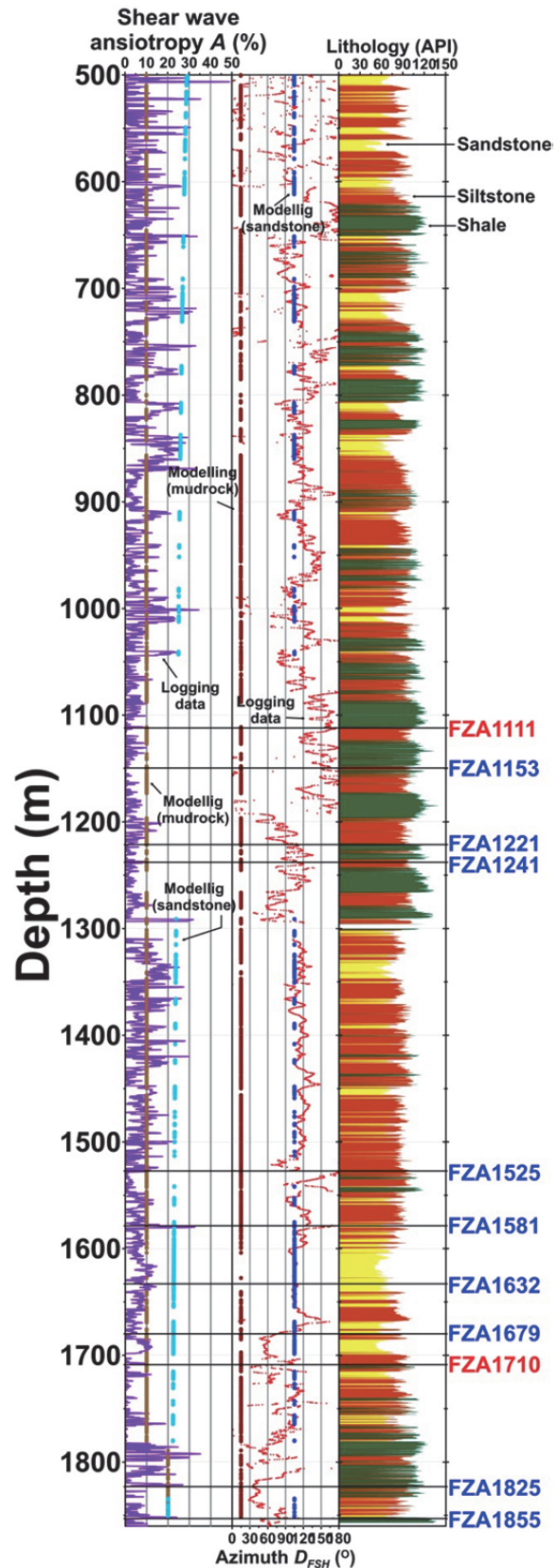


Fig. 5 Calculated and measured anisotropy (velocity anisotropy ratio  $A$  and FSH direction  $D_{FSH}$ ) of the elastic wave velocities.

Table 1 The calculated wave anisotropy of the rock mass around TCDP hole A.

Depth (m)	Lithology	Rock mass (neglecting joints)		Rock mass (considering joints)	
		A (%)	$D_{FSH}$	A (%)	$D_{FSH}$
700-740	sandstone	A (%)	27	A (%)	24
		$D_{FSH}$	105°	$D_{FSH}$	105°
840-856	sandstone	A (%)	26	A (%)	24
		$D_{FSH}$	105°	$D_{FSH}$	106°
856-1012	mudrock	A (%)	5.5	A (%)	5.0
		$D_{FSH}$	15°	$D_{FSH}$	14°
1350-1529	mudrock	A (%)	5.5	A (%)	5.3
		$D_{FSH}$	15°	$D_{FSH}$	14°
1600-1641	sandstone	A (%)	23	A (%)	21
		$D_{FSH}$	105°	$D_{FSH}$	106°
1785-1855	mudrock	A (%)	20	A (%)	20
		$D_{FSH}$	15°	$D_{FSH}$	14°

4. Discussion

4.1 Host rock induced wave anisotropy factors

Based on the measured anisotropy (logging data), lithology is the most important factors inducing wave velocity anisotropy. Furthermore, the depth and dip angle are also dominating factors on the wave velocity anisotropy.

The measured and calculated  $D_{FSH}$  and  $A$  are listed in Fig. 5. The corresponding lithology are also indicated (yellow: sandstone; brown: siltstone; green: shale). Fig. 5 shows that the measured FSH direction  $D_{FSH}$  of sandstone (blue dots) is well predicted ( $D_{FSH}$  is 105° for the dip direction of the bedding plane is 105°; Fig. 6) using the laboratory obtained elastic compliance of intact rocks although the measured one demonstrated spatial variations. Fig. 7 is the histogram of  $D_{FSH}$  (concentrated in about 100° – 120°) measured in sandstone from borehole logging data. That is, the measured  $D_{FSH}$  is well depict only based on the elastic compliance anisotropy of intact rock  $D_{FSH}$ .

The predicted  $D_{FSH}$  of mudrock (siltstone and shale) is 15° (Fig. 5), which is highly deviated from the measured one. However, the measured  $D_{FSH}$  gradually changed below 1785 m and the direction varied from east (90°) to north (0°). This difference is caused by the variation of the dip angle changing from about 30 degree to 60 degree. As indicated in Fig. 3, the anisotropy of the mudrock will increase

with the dip angle of the bedding plane. Above 1785 m, the anisotropy of the mudrocks is too low to obtain an identical  $D_{FSH}$ . For velocity anisotropy ratio increased significantly below 1785 m (purple color, left part of Fig. 3), the measured  $D_{FSH}$  tends to be dominated by the strike of the bedding plane (N15°E), which is illustrated in Fig. 6. The measured anisotropy ratio is close to the calculated ones (20%).

The spatial variation of the measured  $D_{FSH}$  of the sandstones is relatively low. The high anisotropy ratio accounts for the stable  $D_{FSH}$ . Meanwhile, the measured anisotropy ratio support that anisotropy ratio of sandstones will increase with increasing depth (Fig. 4; pink dash line). Based on Fig. 4, the  $A$  decreased from about 30% to 20% when the depth increased from 500 to 1860m (effective confining pressure increased from 6 to 23 MPa if a submerge unit weight of 1.22 g/cm<sup>3</sup> is assumed).

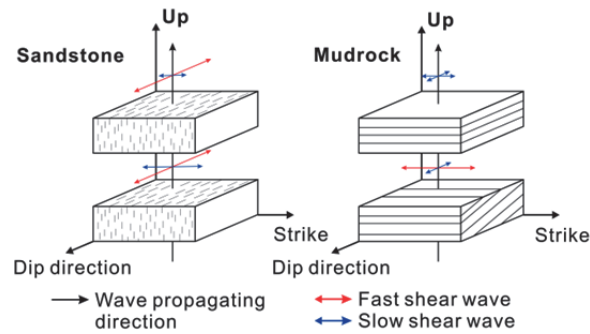


Fig. 6 The sources of wave anisotropy of sandstones and mudrocks.

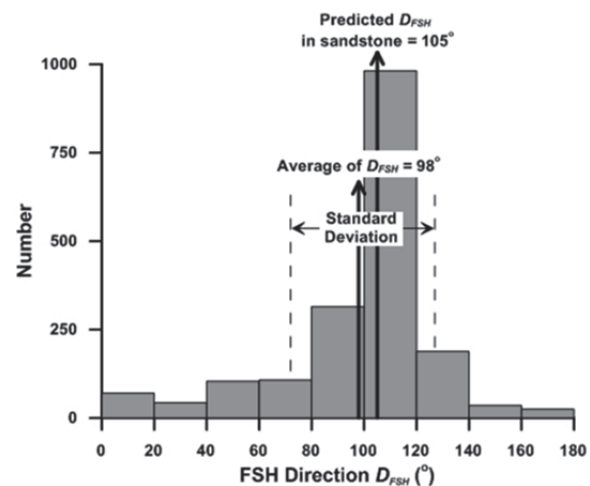


Fig. 7 The histogram of  $D_{FSH}$  measured in sandstone from borehole logging data.

#### 4.2 Influence of Joints on anisotropy of elastic wave velocity

The joint induced wave anisotropy decreases with increasing depth (or stress), which is significant in shallow depth (Boness and Zoback, 2006a). To demonstrate the influence of stress on the anisotropy, the rock mass in the depth interval of 828 – 884m (sandstones here is taken into account an isotropic material) is evaluated. Fig. 8(a) shows the orientations of the joint distributed in the studied depth interval. The parameters used were listed in Table 2.

Table 2 Parameters used in the Oda model.

$r$ (m)	0.2
$h$ (MPa)	360
$g$ (-)	200

Fig. 8(b) shows that the anisotropy ratio is decreased rapidly with increasing depth. It is because that the aperture decreased with increasing confining stress rapidly. Therefore, the compliance tensor of joints  $S_{ijkl}^{(C)}$  becomes smaller than the compliance tensor of host rock  $S_{ijkl}^{(M)}$ . As depth reaches 800 m, the joint induced anisotropy ratio is only 3%. Meanwhile, the predicted wave anisotropy  $A$  is 26% at -800m if the host rock (sandstone) is assumed as a transversely isotropic material. It suggests that the wave anisotropy will be dominated gradually by host rock with increasing depth. In TCDP logging data (Fig. 2), the tendency of wave anisotropy  $A$  gets smaller with depth is because the effect of joints decreases gradually.

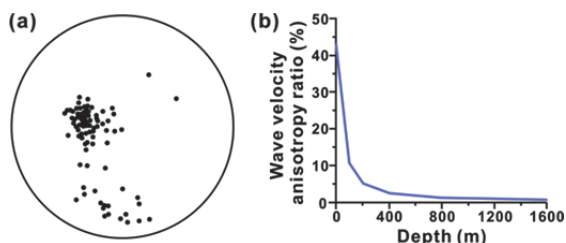


Fig. 8 (a) Orientations of the joints distributed in the depth interval of 828 – 884 m. (b) The velocity anisotropy ratio of rock mass in the studied depth interval.

Besides, the joint length is uncertain in this study because the data are from logging and core. Besides, the vertical resolution of the average transmitter-receive spacing of DSI logger is about 4 meters (Schlumberger, 2004). Therefore, it is possible that the acute variation of  $A$  and  $D_{FSH}$  is caused by local change of joint orientation or existence of longer joint. The Oda model (1986) is only valid for a representative elementary volume (REV) which contains enough number of cracks. The measurement volume of velocity log is less than the REV of the Oda model. We speculate that the model prediction failed to capture the local variation of the wave anisotropy which dominated by the abruptly change of joint characteristics (e.g. length, orientation or joint density).

#### 5. Conclusions

This study used the laboratory wave velocity measurement of intact rocks, equivalent continuum model for describing the elastic compliance of jointed rock mass, and discontinuities data to evaluate the dominating factors of the wave anisotropy. The TCDP borehole A was used as a studied case. Based on the logging data, it is obvious that the wave anisotropy characteristics in sandstone and siltstone are different. The wave anisotropy in sandstone is mainly dominated by confining pressure, but the influence of bedding plane is significant for siltstone.

Based on the anisotropic elastic compliance of sandstones and mudrocks derived from laboratory wave velocity measurement, the calculated wave anisotropy of intact rocks (neglecting the influence of joints) generally comparable to the measured anisotropy from borehole velocity logs. The measured FSH directions of sandstones could be dominated by the micro fractures perpendicular to the bedding planes. When the dip angles become steeper (in a depth greater than 1785 m), the measured FSH directions of mudrocks seems dominated by the dip direction of bedding planes. It suggests that the inherent anisotropy of intact rocks accounts for the wave anisotropy.

Relatively, the influence of joints is insignificant using the Oda model and assumed parameters, especially at a depth greater than 500 m. However, the discontinuities separate the source and receiver of the velocity logging could explain the scatters of the measured FSH directions and the wave velocity anisotropy ratio.

To conclude, determining the direction of the maximum horizontal principal stress from the

direction of the fast horizontal shear wave velocity should carefully consider the influence of inherent anisotropy of rock mass.

### Acknowledgements

The authors are grateful to the support from MOST, Taiwan. The project numbers are MOST 103-2116-M-008-005 and 104-3113-M-008-001.

### References

- Alford, R.M. (1986): Shear data in the presence of azimuthal anisotropy, Annual International Meeting of the Society of Exploration Geophysicists Expanded Abstracts, Vol. 56, pp. 476–479.
- Brie, A., Endo, T. and Hoyle, D. (1998): New directions in sonic logging, *Oilfield Review*, Vol. 10, pp. 40–55.
- Boness, N.L. and Zoback, M.D. (2004): Stress-induced seismic velocity anisotropy and physical properties in the SAFOD Pilot Hole in Parkfield, CA, *Geophysical Research Letters*, Vol. 31, doi: 10.1029/2003GL019020.
- Boness, N.L. and Zoback, M.D. (2006a): A multiscale study of the mechanisms controlling shear velocity anisotropy in the San Andreas Fault Observatory at Depth, *Geophysics*, Vol. 71, No. 5, doi:10.1190/1.2231107
- Boness, N.L. and Zoback, M.D. (2006b): Mapping stress and structurally controlled crustal shear velocity anisotropy in California, *Geological Society of America*, Vol. 34, No.10, pp. 825-828.
- Castagna, P., Batzle, M. L., and Eastwood, R. L. (1985): Relationships between compressional-wave and shear-wave velocities in elastic silicate rocks, *Geophysics*, Vol. 50(4), pp. 571-581.
- Cheng, Y.C. (2006): Inherent and stress-dependent anisotropy of permeability for jointed rock masses, Master thesis, National Central University.
- Haimson, B., Lin, W., Oku, H., Hung, J.-H. and Song, S.-R. (2010): Integrating borehole-breakout dimensions, strength criteria, and leak-off test results, to constrain the state of stress across the Chelungpu Fault, Taiwan, *Tectonophysics*, Vol. 482, pp. 65–72.
- Hung, J.H., Ma, K.F., Wang, C.Y., Ito, H., Lin, W. and Yeh, E.C. (2009): Subsurface structure, physical properties, fault-zone characteristics and stress state in scientific drill holes of Taiwan Chelungpu Fault Drilling Project, *Tectonophysics*, Vol. 466, pp. 307–321.
- Lin, W., Yeh, E.C., Ito, H., Hirono, T., Soh, W., Wang, C.Y., Ma, K.F., Hung, J.H. and Song, S.R. (2007): Preliminary results of stress measurement using drill cores of TCDP Hole-A: an application of anelastic strain recovery method to three dimensional in-situ stress determination, *Terrestrial, Atmospheric and Oceanic Sciences*, Vol. 18, No. 2, pp. 379–393.
- Louis, L., Chen, N.T.M., David, C., Robion, P., Wong, T.F. and Song, S.R. (2008): Anisotropy of magnetic susceptibility and P-wave velocity in core samples from the Taiwan Chelungpu-Fault Drilling Project (TCDP), *Journal of Structural Geology*, Vol. 30, pp. 948–962.
- Louis, L., David, C. Spacek, P., Wang, T.F., Fortin, J. and Song, S.R. (2012): Elastic anisotropy of core samples from the Taiwan Chelungpu Fault Drilling Project (TCDP): direct 3-D measurements and weak anisotropy approximations, *Geophysical Journal International*, Vol. 188, pp. 239–252.
- Mueller, M.C. (1991): Prediction of lateral variability in fracture intensity using multicomponent shear-wave seismic as a precursor to horizontal drilling, *Geophysical Journal International*, Vol. 107, pp. 409–415.
- Musgrave, M.J.P. (1971): *Crystal acoustics*, Holden-day, San Francisco.
- Oda M. (1986): An equivalent continuum model for coupled stress and fluid flow analysis in jointed rock masses, *Water Resources Res.*, Vol. 22, No. 13, pp. 1845-1856.
- Oda, M. (1988): An experimental study of the elasticity of mylonite rock with random cracks, *International Journal of Rock Mechanics and Mining Sciences & Geomechanics Abstracts*, Vol 25, No. 2, pp. 59-69.
- Sayers, C.M. (1994): The elastic anisotropy of shales, *Journal of Geophysical Research*, Vol. 99, pp. 767–774.
- Schlumberger (2004): DSI dipole shear sonic imager, Schlumberger marketing communications, Houston., 2004
- Wu, Y.H., Yeh, E.C., Dong, J.J., Kuo, L.W., Hsu, J.Y. and Hung, J.H. (2008): Core-log integration studies in hole-A of Taiwan Chelungpu-fault Drilling Project, *Geophysical Journal International*, Vol. 174, pp. 949-965.
- Yabe, Y., Song, S. R. and Wang, C. Y. (2008): In-situ stress at the northern portion of the Chelungpu fault, Taiwan, estimated on boring cores recovered from a 2-km-deep hole of TCDP, *Earth Planets Space*, Vol. 60, pp. 809–819.
- Yeh, E.C., Sone, H., Nakaya, T., Ian, K.H., Song, S.R., Hung, J.H., Lin, W., Hirono, T., Wang, C.Y., Ma, K.F., Soh, W. and Kinoshita, M. (2007): Core description and characteristics of fault zones from Hole-A of the Taiwan Chelungpu-Fault drilling project, *Terrestrial, Atmospheric and Oceanic Sciences*, Vol. 18, No. 2, pp. 327–357.